Volume 7 | Number 12 | 28 March 2015 | Pages 5063–5548

Nanoscale

www.rsc.org/nanoscale

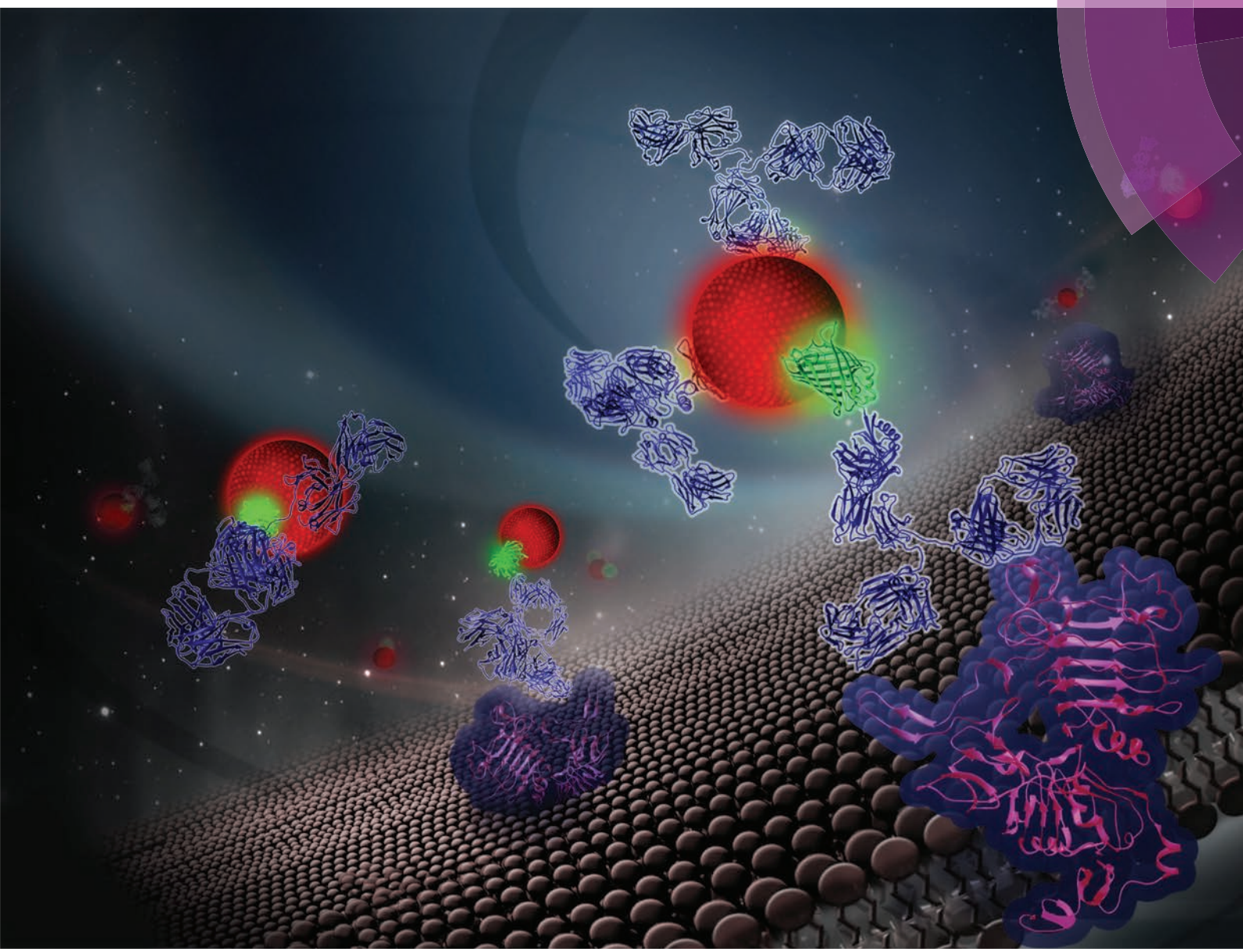

ISSN 2040-3364

ROYAL SOCIETY OF CHEMISTRY

COMMUNICATION

Akira Sasaki, Takashi Jin *et al.*

Recombinant protein (EGFP-Protein G)-coated PbS quantum dots for *in vitro* and *in vivo* dual fluorescence (visible and second-NIR) imaging of breast tumors

NCNST

Nanoscale

COMMUNICATION

View Article Online
View Journal | View Issue

Cite this: *Nanoscale*, 2015, **7**, 5115

Received 4th November 2014,
Accepted 18th December 2014

DOI: 10.1039/c4nr06480a

www.rsc.org/nanoscale

Recombinant protein (EGFP-Protein G)-coated PbS quantum dots for *in vitro* and *in vivo* dual fluorescence (visible and second-NIR) imaging of breast tumors†

Akira Sasaki,*[a,b] Yoshikazu Tsukasaki,‡[b] Akihito Komatsuzaki,[b] Takao Sakata,[c] Hidehiro Yasuda[c] and Takashi Jin*[b,d,e]

We report a one-step synthetic strategy for the preparation of recombinant protein (EGFP-Protein G)-coated PbS quantum dots for dual (visible and second-NIR) fluorescence imaging of breast tumors at the cellular and whole-body level.

Non-invasive whole-body imaging using near-infrared (NIR) fluorescence has been broadly developed because of its low tissue absorption and scattering compared to that observed with visible fluorescence.[1–3] Recently, second-NIR fluorescence (1000–1500 nm) has been used for non-invasive *in vivo* imaging.[4–7] Second-NIR fluorescence imaging has advantages over traditional NIR fluorescence imaging (700–900 nm) such as reduced light scattering and minimal autofluorescence.[5] For the second-NIR fluorescence imaging, semiconductor quantum dots (QDs) such as PbS,[8–13] PbSe,[10] and Ag_2S[14] are promising fluorescent probes because of their strong fluorescence and photostability at wavelengths in the range of 1000–1500 nm. However, fluorescence imaging using second-NIR QDs usually encounters two major difficulties. First, the preparation of the QD-based fluorescent probe needs multiple synthetic steps such as QD formation, surface modification and biomolecule conjugation.[8–14] Second, the fluorescence detectors of conventional microscope systems do not support second-NIR fluorescence imaging.[5,6,15,16] To overcome these problems, we have developed a dual (visible and second-NIR) emission QD probe that can be used for both cellular and non-invasive whole-body imaging. In this communication, we report a facile synthesis of recombinant protein functionalized PbS QDs with dual emission (visible and second-NIR fluorescence), which have a binding ability for antibody molecules (IgG) in aqueous solution.

We have used an enhanced green fluorescent protein (EGFP)-Protein G B1 domain[17] tagged with glutathione *S*-transferase (GST) as a template[18,19] (GST-EGFP-GB1; 61.7 kDa, see ESI†) to grow PbS QDs in the aqueous phase (Scheme 1). The recombinant protein, GST-EGFP-GB1 was genetically designed and prepared by a conventional method for recombinant protein synthesis in *Escherichia coli*. Protein G is a cell surface protein of *Streptococcus* and its B1 domain binds to the Fc region of immunoglobulin G (IgG). It has been widely used for detecting and purifying IgG antibodies.[17] Particularly in cancer molecular imaging, a receptor-targeting antibody can act as a powerful tool *via* the conjugation of antibodies to the QD surface. In this case, a large amount of antibodies was used for conjugation to QDs.[2,11,13] Since the GST-EGFP-GB1-coated QDs contain a protein G B1 domain, they can easily bind to antibody molecules by a simple mixing of antibodies with the QD solution.[20–22] The fluorescent protein EGFP is chosen to add a function of visible fluorescence emission to the second-NIR emitting PbS QDs. This dual-emitting property of the QDs enables a conduction of high-resolution cellular confocal imaging by EGFP fluorescence in addition to the deep-tissue imaging by second-NIR fluorescence. Thus the GST-EGFP-GB1-coated QDs make it possible to correlate the intracellular localization of probes with bio-distribution in the whole mouse body.

GST-EGFP-GB1-coated PbS QDs can be prepared by using a protein-mediated QD synthetic method (Scheme 1).[18,19] The synthesis is carried out by reacting GST-EGFP-GB1 with lead acetate ($Pb(Ac)_2$) under ambient conditions to promote the binding of Pb^{2+} to GST-EGFP-GB1 (see the Experimental section in ESI†). The addition of an aqueous solution of sodium sulfide (Na_2S) immediately forms PbS QDs coated with

[a]*Biomedical Research Institute, National Institute of Advanced Industrial Science and Technology (AIST), Tsukuba, Ibaraki 305-8566, Japan. E-mail: akira.sasaki@aist.go.jp*
[b]*Laboratory for Nano-Bio Probes, Quantitative Biology Center, RIKEN, Suita, Osaka 565-0874, Japan. E-mail: tjin@riken.jp*
[c]*Research Center for Ultra-High Voltage Electron Microscopy, Osaka University, Ibaraki, Osaka 567-0047, Japan*
[d]*WPI Immunology Frontier Research Center, Osaka University, Suita, Osaka 565-0871, Japan*
[e]*Graduate School of Frontier Biosciences, Osaka University, Suita, Osaka 565-0871, Japan*
† Electronic supplementary information (ESI) available. See DOI: 10.1039/c4nr06480a
‡ Present address: University of Texas Health Science Center Northeast, Tyler, Texas 75708-3154, USA.

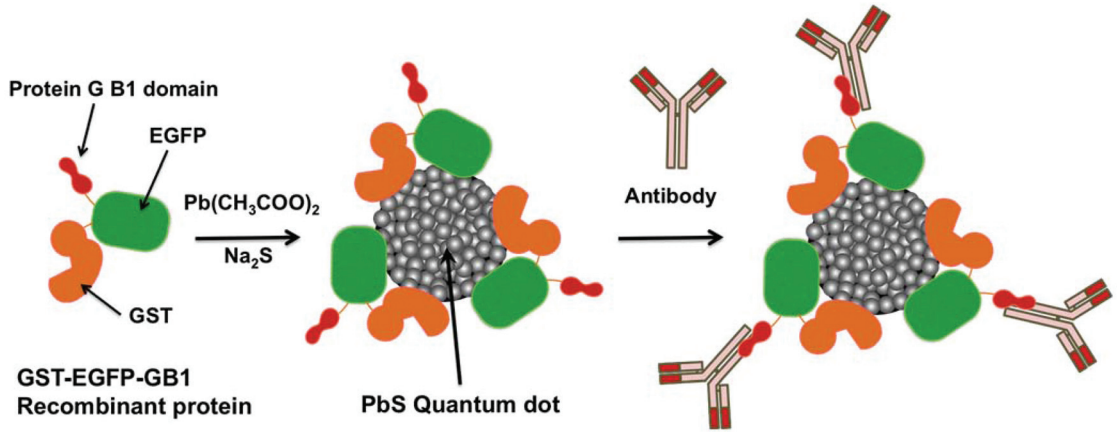

Scheme 1 A schematic representation of the synthesis of recombinant protein (GST-EGFP-GB1)-coated PbS QDs. GST-EGFP-GB1 protein is used as a template for growing PbS QDs in the aqueous phase. Antibody molecules bind to the protein G B1 domain on the QD by simply mixing the antibody with the QD solution.

the GST-EGFP-GB1 protein. By this synthetic method, we can easily prepare protein-coated PbS QDs within 10 minutes. To characterize the GST-EGFP-GB1-coated PbS QDs, we have analysed their transmission electron microscopic (TEM) images, dynamic light scattering (DLS), and fluorescence/absorption spectra. Fig. 1a shows TEM images of GST-EGFP-GB1-coated PbS QDs. The PbS QDs have spherical shapes (*ca.* 5 nm) with a selected area electron diffraction (SAED) pattern and lattice fringes, confirming the crystalline nature of the PbS QDs with a cubic structure.[23] The hydrodynamic size of the PbS QDs was determined to be *ca.* 30 nm in diameter by DLS (Fig. 1b). This value is *ca.* 25 nm larger than that determined by TEM analysis. This indicates that the GST-EGFP-GB1 fusion proteins (10 nm in diameter) surround the surface of the PbS QDs. The fluorescence spectrum of the GST-EGFP-GB1-coated PbS QDs showed dual emission, with the visible emission at 515 nm and a second-NIR emission at 1150 nm, under excitation at 450 nm (Fig. 1c and S1, S2 in ESI†). The visible and NIR fluorescence emissions are from EGFP proteins and PbS QDs, respectively. The quantum yield (QY) of the second-NIR fluorescence of PbS QDs (1150 nm emission peak) was measured by a relative method with CdSeTe/CdS QDs (840 nm emission, QY = 50%) as a standard (see the Experimental section in ESI†). QY was determined to be 10% in water.

The binding ability of GST-EGFP-GB1-coated QDs towards antibody was confirmed using fluorescence correlation spectroscopy (FCS).[23,24] Fig. 2 shows fluorescence autocorrelation curves for the GST-EGFP-GB1 protein, GST-EGFP-GB1-coated QD, and the mixture of anti-HER2 (human epidermal growth factor 2) antibody + GST-EGFP-GB1-coated QDs. Fluorescence autocorrelation curves are fitted according to the one-component diffusion model,[23,24] allowing spherical shape assump-

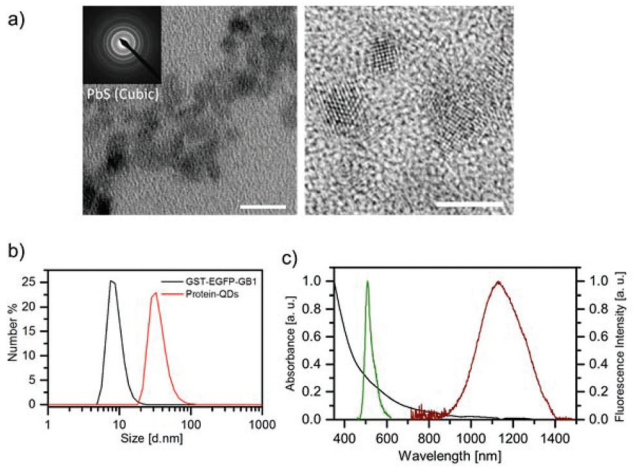

Fig. 1 (a) TEM image of protein (GST-EGFP-GB1)-coated PbS QDs (scale bar: 10 nm). The inset shows the SAED pattern of the QDs. The right image shows a high-resolution TEM image of the PbS QDs (scale bar: 5 nm). (b) Distribution of the hydrodynamic diameter of free GST-EGFP-GB1 protein and the QDs measured by DLS. (c) Absorption (black) and fluorescence spectra of the protein-coated QDs with emission peaks at 515 nm (EGFP; green) and 1150 nm (QD; red).

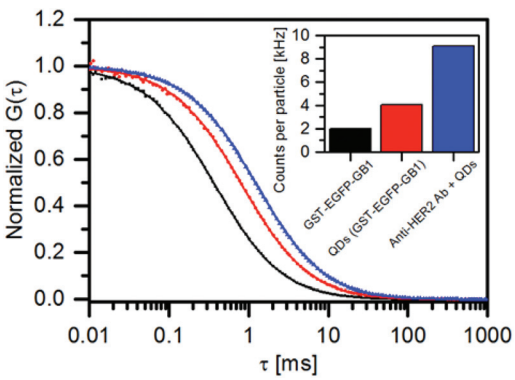

Fig. 2 Fluorescence autocorrelation curves of the GST-EGFP-GB1 protein (black), GST-EGFP-GB1-coated QDs (red), and the mixture of anti-HER2 antibody and the QDs (blue). The inset graph shows photon counts per particle (CPP) value of the samples calculated from fluorescence correlation spectroscopy (FCS).

tion for all three samples. Binding between the Protein G B1 domain and the antibody was confirmed by the change in the diffusion time of the GST-EGFP-GB1-coated QDs (0.82 ms) and a mixture of anti-HER2 antibody + GST-EGFP-GB1-coated QDs (1.26 ms). Based on the Einstein–Stokes equation, hydrodynamic diameters were estimated to be 23 nm for GST-EGFP-GB1-coated QDs and 35 nm for the anti-HER2 antibody + GST-EGFP-GB1-coated QDs complex. This result confirms the binding of anti-HER2 antibody to the GST-EGFP-GB1-coated QDs. It is also confirmed by the analysis of the photon counts per particle (CPP), expressing the fluorescence brightness of the single-particle. The CPP value of the GST-EGFP-GB1-coated QDs is two times higher than that of the free GST-EGFP-GB1 protein (inset of Fig. 2), indicating that at least two GST-EGFP-GB1 molecules are included in one PbS QD. It should also be noted that the CPP value of the mixture of anti-HER2 antibody + GST-EGFP-GB1-coated QDs is four times higher than that of the free GST-EGFP-GB1 protein. This indicates that the complex of antibody + QDs contain two GST-EGFP-GB1-coated QDs due to the inter-particle binding of the GB1 domain by their respective QDs.

To demonstrate the capability of GST-EGFP-GB1-coated QDs, we first performed the fluorescence imaging of breast tumor cells in the visible and second-NIR regions. For fluorescence imaging, we have used a human breast tumor cell line (KPL-4)[25] over-expressing HER2 on its cell membrane. Fig. 3a shows a high-resolution confocal fluorescence image (excitation: 473 nm, emission: 515 nm, at 60× magnification) of KPL-4 cells stained with anti-HER2 antibody and GST-EGFP-GB1-coated QDs. Green fluorescence of the EGFP is clearly observed on the cell surface, indicating that GST-EGFP-GB1-coated QDs bind to the HER2 receptors *via* anti-HER2 antibody on the KPL-4 cell surface (Fig. 3a and S3 in ESI†). For the second-NIR fluorescence imaging, we have used a home-built wide-field dissecting microscope equipped with an InGaAs detector (see the Experimental section in ESI†). Fig. 3b shows a second-NIR fluorescence image of KPL-4 cells stained with anti-HER2 antibody and GST-EGFP-GB1-coated QDs. The second-NIR fluorescence (excitation: 670 nm, emission: 1300 nm, 6.3× magnification) is clearly observed after a 30 min incubation of KPL-4 cells with anti-HER2 antibody and GST-EGFP-GB1-coated QDs (Fig. 3b). Each bright spot represents a single-cell. These results show that the GST-EGFP-GB1-coated QDs act as a dual-emission molecular targeting probe with visible and second-NIR fluorescence. GST-EGFP-GB1-coated QDs showed low cytotoxicity in HeLa cells at the concentration (<250 nM) used for *in vitro* and *in vivo* fluorescence imaging (Fig. S4 in ESI†).

Next, we performed a second-NIR fluorescence imaging of the breast tumor implanted KPL-4 cells in a nude mouse. An aqueous solution (200 μL) of GST-EGFP-GB1-coated QDs (1 μM) mixed with anti-HER2 antibody was injected into the tail vein of a live mouse, and second-NIR fluorescence images (excitation: 670 nm, emission: 1300 nm) were taken after 48 hours of QD injection (Fig. 4). As shown in Fig. 4c, intense second-NIR fluorescence from the breast tumor is clearly observed, compared to the control without QD injection (Fig. S5 in ESI†). This indicates the accumulation of anti-HER2 antibody binding QDs in the tumor. In contrast, there is no

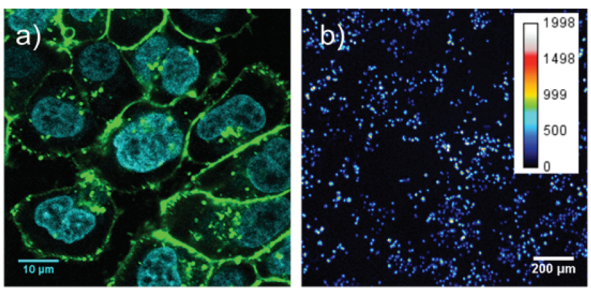

Fig. 3 Fluorescence imaging of breast tumor cells (KPL-4). (a) Conventional laser scanning confocal microscopic image (515 nm, green) of cells after the incubation of anti-HER2 antibody, followed by the incubation with QDs (60× magnification oil immersion objective). Cell nucleus was stained with the Hoechst 33342 reagent (cyan). (b) Second-NIR fluorescence image (1300 nm) of KPL-4 after the incubation of anti-HER2 antibody, followed by incubation with the QDs (6.3× magnification objective).

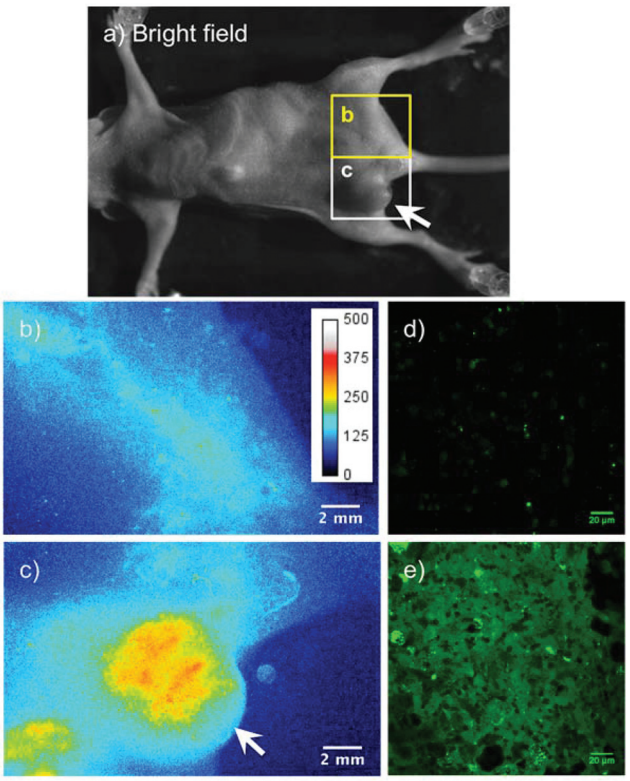

Fig. 4 Second-NIR fluorescence images (1300 nm) of a breast tumor after injection of GST-EGFP-GB1 protein-coated PbS QDs mixed with anti-HER2 antibody. (a) Bright field image of a nude mouse breast cancer tumor xenograft. Second-NIR fluorescence image is obtained in the region (b) as a negative control and (c) as a breast tumor. The location of the breast tumor is indicated by the arrows in the bright field image (a) and fluorescence image (c). *Ex vivo* confocal microscopy images (515 nm) of (d) the breast tumor without QD injection (negative control) and (e) the breast cancer tumor 48 h after QD injection.

significant second-NIR fluorescence in the area without tumors (Fig. 4b). To confirm actual accumulation of the QDs in the breast tumor cells, we carried out *ex vivo* fluorescence imaging of an isolated tumor at a higher magnification by a confocal microscope and a second-NIR microscope (Fig. 4d, e, and S6 in ESI†). Compared with the negative control without QDs injection (Fig. 4d), intense fluorescence of EGFP emitting from the anti-HER2 antibody-conjugated QDs was observed in the breast tumor (Fig. 4e). This finding indicates that the conjugates of anti-HER2 antibody and GST-EGFP-GB1-coated QDs pass through the blood vessels of the breast tumor and bind to the HER2 receptors on the tumor cells.

In summary, we have demonstrated a one-step facile method for preparing GST-EGFP-GB1 protein-coated PbS QDs with a dual emission of visible (515 nm) and second-NIR fluorescence (1150 nm). The PbS QDs have two molecules of GST-EGFP-GB1 protein per QD particle, and they can easily bind IgG antibodies *via* their GB1 domain. We have demonstrated that the GST-EGFP-GB1-coated PbS QDs have a dual-color probe capability for the fluorescence molecular imaging of breast tumors at the cellular and whole-body level. An important feature of this work is that the GST-EGFP-GB1-coated QDs make it possible to correlate the cellular distribution of QD probes with their bio-distribution in the whole body. These dual emission PbS QDs with antibody binding ability can be extended to a variety of *in vitro* and *in vivo* tumor imaging techniques by constructing conjugates between specific antibodies for tumors and the GST-EGFP-GB1 protein-coated PbS QDs.

Acknowledgements

We thank Dr Scott Gradia (University of California, Berkeley) for making the Addgene plasmid 29713 available through Addgene. All experiments were performed in compliance with the National Institutes of Health Guidelines for the Care and Use of Laboratory Animals and were approved by the Osaka University Animal Care and Use Committee.

Notes and references

1 (*a*) R. Weissleder, *Nat. Biotechnol.*, 2001, **19**, 316–317; (*b*) J. V. Frangioni, *Curr. Opin. Chem. Biol.*, 2003, **7**, 626–634; (*c*) X. Gao, Y. Cui, R. M. Levenson, L. W. K. Chung and S. Nie, *Nat. Biotechnol.*, 2004, **22**, 969–976; (*d*) S. Kim, Y. T. Lim, E. G. Soltesz, A. M. De Grand, D. J. Lee, A. Nakayama, J. A. Parker, T. Mihaljevic, R. G. Laurence, D. M. Dor, L. H. Cohn, M. G. Bawendi and J. V. Frangioni, *Nat. Biotechnol.*, 2004, **22**, 93–97; (*e*) X. Gao, L. Yang, J. A. Petros, F. F. Marshall, J. W. Simons and S. Nie, *Curr. Opin. Biotechnol.*, 2005, **16**, 63–72; (*f*) C. L. Amiot, S. Xu, S. Liang, L. Pan and J. X. Zhao, *Sensors*, 2008, **8**, 3082–3105.

2 X. He, J. Gao, S. S. Gambhir and Z. Cheng, *Trends Mol. Med.*, 2010, **16**, 574–583.

3 J. H. Ryu, M. Shin, S. A. Kim, S. Lee, H. Kim, H. Koo, B. S. Kim, H. K. Song, S. H. Kim, K. Choi, I. C. Kwon, H. Jeon and K. Kim, *Biomaterials*, 2013, **34**, 9149–9159.

4 A. M. Smith, M. C. Mancini and S. Nie, *Nat. Nanotechnol.*, 2009, **4**, 710–711.

5 N. Won, S. Jeong, K. Kim, J. Kwag, J. Park, S. G. Kim and S. Kim, *Mol. Imaging*, 2012, **11**, 338–352.

6 L. A. Sordillo, Y. Pu, S. Pratavieira, Y. Budansky and R. R. Alfano, *J. Biomed. Opt.*, 2014, **19**, 056004.

7 (*a*) Z. Liu, W. Cai, L. He, N. Nakayama, K. Chen, X. Sun, X. Chen and H. Dai, *Nat. Nanotechnol.*, 2007, **2**, 47–52; (*b*) K. Welsher, Z. Liu, D. Daranciang and H. Dai, *Nano Lett.*, 2008, **8**, 586–590; (*c*) K. Welsher, Z. Liu, S. P. Sherlock, J. T. Robinson, Z. Chen, D. Daranciang and H. Dai, *Nat. Nanotechnol.*, 2009, **4**, 773–780; (*d*) K. Welsher, S. P. Sherlock and H. Dai, *Proc. Natl. Acad. Sci. U. S. A.*, 2011, **108**, 8943–8948; (*e*) G. Hong, J. C. Lee, J. T. Robinson, U. Raaz, L. Xie, N. F. Huang, J. P. Cooke and H. Dai, *Nat. Med.*, 2012, **18**, 1841–1846; (*f*) J. T. Robinson, G. Hong, Y. Liang, B. Zhang, O. K. Yaghi and H. Dai, *J. Am. Chem. Soc.*, 2012, **134**, 10664–10669; (*g*) Z. Tao, G. Hong, C. Shinji, C. Chen, S. Diao, A. L. Antaris, B. Zhang, Y. Zou and H. Dai, *Angew. Chem., Int. Ed.*, 2013, **125**, 13240–13244; (*h*) D. J. Naczynski, M. C. Tan, M. Zevon, B. Wall, J. Kohl, A. Kulesa, S. Chen, C. M. Roth, R. E. Riman and P. V. Moghe, *Nat. Commun.*, 2013, **4**, 2199, DOI: 10.1038/ncomms3199.

8 E. H. Sargent, *Adv. Mater.*, 2005, **17**, 515–522.

9 M. A. Hines and G. D. Scholes, *Adv. Mater.*, 2003, **15**, 1844–1849.

10 (*a*) B. R. Hyun, H. Chen, D. A. Rey, F. W. Wise and C. A. Batt, *J. Phys. Chem. B*, 2007, **111**, 5726–5730; (*b*) J. M. Pietryga, D. J. Werder, D. J. Williams, J. L. Casson, R. D. Schaller, V. I. Klimov and J. A. Hollingsworth, *J. Am. Chem. Soc.*, 2008, **130**, 4879–4885.

11 Y. Nakane, Y. Tsukasaki, T. Sakata, H. Yasuda and T. Jin, *Chem. Commun.*, 2013, **49**, 7584–7586.

12 Y. Tsukasaki, M. Morimatsu, G. Nishimura, T. Sakata, H. Yasuda, A. Komatsuzaki, T. M. Watanabe and T. Jin, *RSC Adv.*, 2014, **4**, 41164–41171.

13 Y. Tsukasaki, A. Komatsuzaki, Y. Mori, Q. Ma, Y. Yoshioka and T. Jin, *Chem. Commun.*, 2014, **50**, 14356–14359.

14 (*a*) Y. Du, B. Xu, T. Fu, M. Cai, F. Li, Y. Zhang and Q. Wang, *J. Am. Chem. Soc.*, 2010, **132**, 1470–1471; (*b*) G. Hong, J. T. Robinson, Y. Zhang, S. Diao, A. L. Antaris, Q. Wang and H. Dai, *Angew. Chem., Int. Ed.*, 2012, **124**, 9956–9959; (*c*) P. Jiang, Z. Q. Tian, C. N. Zhu, Z. L. Zhang and D. W. Pang, *Chem. Mater.*, 2012, **24**, 3–5; (*d*) Y. Zhang, G. Hong, Y. Zhang, G. Chen, F. Li, H. Dai and Q. Wang, *ACS Nano*, 2012, **6**, 3695–3702; (*e*) P. Jiang, C. N. Zhu, Z. L. Zhang, Z. Q. Tian and D. W. Pang, *Biomaterials*, 2012, **33**, 5130–5135; (*f*) H. Y. Yang, Y. W. Zhao, Z. Y. Zhang, H. M. Xiong and S. N. Yu, *Nanotechnology*, 2013, **24**, 055706; (*g*) Y. Zhang, Y. Zhang, G. Hong, W. He, K. Zhou,

K. Yang, F. Li, G. Chen, Z. Liu, H. Dai and Q. Wang, *Biomaterials*, 2013, **34**, 3639–3646; (*h*) Y. Zhang, Y. Liu, C. Li, X. Chen and Q. Wang, *J. Phys. Chem. C*, 2014, **118**, 4918–4923; (*i*) R. Gui, A. Wan, X. Liu, W. Yuan and H. Jin, *Nanoscale*, 2014, **6**, 5467–5473; (*j*) C. Li, Y. Zhang, M. Wang, Y. Zhang, G. Chen, L. Li, D. Wu and Q. Wang, *Biomaterials*, 2014, **35**, 393–400; (*k*) G. Chen, F. Tian, Y. Zhang, Y. Zhang, C. Li and Q. Wang, *Adv. Funct. Mater.*, 2014, **24**, 2481–2488.

15 G. Wang, J. Ji and X. Xu, *J. Mater. Chem. C*, 2014, **2**, 1977–1981.

16 S. K. Patel, M. J. Patrick, J. A. Pollock and J. M. Janjic, *J. Biomed. Opt.*, 2013, **18**, 101312.

17 A. M. Gronenborn, D. R. Filpula, N. Z. Essig, A. Achari, M. Whitlow, P. T. Wingfield and G. M. Clore, *Science*, 1991, **253**, 657–661.

18 N. Ma, A. F. Marshall and J. Rao, *J. Am. Chem. Soc.*, 2010, **132**, 6884–6885.

19 X. He, L. Gao and N. Ma, *Sci. Rep.*, 2013, **3**, 2825.

20 R. Elshafey, A. C. Tavares, M. Siaj and M. Zourob, *Biosens. Bioelectron.*, 2013, **50**, 143–149.

21 T. Niide, K. Shimojo, R. Wakabayashi, M. Goto and N. Kamiya, *Langmuir*, 2013, **29**, 15596–15605.

22 X. Sun, G. Zhang, R. S. Keynton, M. G. O'Toole, D. Patel and A. M. Gobin, *Nanomedicine*, 2013, **9**, 1214–1222.

23 T. Jin, F. Fujii, Y. Komai, J. Seki, A. Seiyama and Y. Yoshioka, *Int. J. Mol. Sci.*, 2008, **9**, 2044–2061.

24 A. Sasaki, H. Sakata and M. Kinjo, *Curr. Pharm. Biotechnol.*, 2010, **11**, 117–121.

25 J. Kurebayashi, T. Otsuki, C. K. Tang, M. Kurosumi, S. Yamamoto, K. Tanaka, M. Mochizuki, H. Nakamura and H. Sonoo, *Br. J. Cancer*, 1999, **79**, 707–717.